Deembedding Static Nonlinearities and Accurately Identifying and Modeling Memory Effects in Wide-Band RF Transmitters

Taijun Liu, *Student Member, IEEE*, Slim Boumaiza, *Member, IEEE*, and Fadhel M. Ghannouchi, *Senior Member, IEEE*

***Abstract*—In this paper, a robust modeling technique for memoryless wide-band radio frequency transmitters using a dynamic exponential weighted moving average algorithm is developed and tested. To improve the relatively limited accuracy of the conventional Wiener model in predicting the response of dynamic nonlinear transmitters, a new augmented Wiener model is proposed along with its parameter-identification procedure. The accuracy of the augmented Wiener model is compared with that of the conventional Wiener model by using an L-band 60-W peak-envelope-power GaAs field-effect-transistor push–pull amplifier-based transmitter, which is driven by a two-carrier wide-band code-division multiple-access signal.**

***Index Terms*—Augmented Wiener model, dynamic exponential weighted moving average, memory effects, wide-band transmitters, Wiener model.**

I. Introduction

THE DESIGN of the RF front-end of third-generation (3G) and beyond wireless communications transceivers is currently an extremely complicated task since it involves numerous criteria that are usually inconsistent. Although the main objective remains ensuring a good quality of signal at the receiver side, the optimization of the channel capacity (in bits per hertz) is also a challenging assignment. This is particularly relevant in the context of wide-band and highly varying envelope signals, as in the cases of multicarrier code-division multiple-access and orthogonal frequency-division multiplexing, where the coexistence of linear and nonlinear distortion sources in the RF transmitter chains compromises their performances in terms of error vector magnitude and adjacent channel power ratio (ACPR). The minimization of the effects of such distortion sources relies primarily on accurate modeling of the RF transmitters.

In the literature, one can distinguish several topologies that were applied to the modeling of dynamic nonlinear systems. For example, Schetzen [1] utilized Volterra series to model nonlinear power amplifiers with memory effects. However, the use of such series-based models is restricted to weak nonlinear systems. Since the models require a high-order kernel, which, in turn, yields high computational complexity, difficulties are often encountered during the model identification procedure when systems are driven by wide-band signals. Although the truncated Volterra series model is considered a good means of resolving the computational complexity [2], this model suffers from the difficulty of real-time implementation. Liu *et al.* [3] proposed a real-valued time-delay neural network to establish a dynamic behavioral model of 3G power amplifiers. Although this new architecture largely simplifies the model topology, it undergoes a relatively slow convergence of the back-propagation algorithm, which was employed to extract the model parameters.

Silva *et al.* presented a nonlinearity filter structure to model a wide-band power amplifier, and applied a polyspectral technique for its identification [4], [5]. The principal part of such a model consists of either a filter nonlinearity or a nonlinearity filter in parallel with another linear filter. The authors mentioned the superiority of this model over a conventional two-box Weiner model (linear + nonlinear) in predicting the response of traveling-wave-tube amplifiers. Despite the closed-form expressions used in the identification of the model parameters, the required measurement data are difficult to collect in an adaptive context. Indeed, it requires a vector network analyzer (VNA) for determining the memoryless part of the model and the frequency transfer function of one of the linear filters. In addition, the memoryless characteristics of the power amplifier under a modulated signal with a high peak-to-average ratio (PAR) differ from the measured characteristics under a continuous-wave signal [6].

In [7], Clark *et al.* reported a two-box model approach—a Wiener system [1] that consists of a two-block structure. The first block represents a linear autoregressive moving average filter that accounts for the memory effects, and the second block denotes a conventional Bessel series model that is used to represent the memoryless nonlinearity. Such a topology can easily deal with strong nonlinearity, but the identification procedure suggested by the authors is difficult to implement under real field conditions since it requires an initial estimation of the autoregressive moving average filter coefficients through a frequency-domain measurement under a small-signal condition using a VNA. Alternatively, in [8], Crama and Rolain proposed a method that estimates the Wiener and Hammerstein structures based on a frequency-domain identification procedure using

Manuscript received April 4, 2005; revised June 9, 2005 and July 13, 2005. This work was supported by the Natural Sciences and Engineering Research Council of Canada.

T. Liu is with the Poly-Grames Research Center, Electrical Engineering Department, École Polytechnique de Montréal, Montréal, QC, Canada H3T 1J4 (e-mail: taijun.liu@polymtl.ca).

S. Boumaiza and F. M. Ghannouchi are with the Intelligent RF Radio Laboratory, Electrical and Computer Engineering Department, University of Calgary, Calgary, AB, Canada T2N 1N4 (e-mail: sboumaiz@ucalgary.ca; fghannou@ucalgary.ca).

Digital Object Identifier 10.1109/TMTT.2005.857105

0018-9480/$20.00 © 2005 IEEE

Petitioners Exhibit 1004
Page 1 of 10

special multisine signals. However, the accuracy of the identification method is greatly compromised by the phase difference between the two channels used to sample the input and output of the device-under-test. Although a relative calibration can be applied with the assumption that one of the two channels is perfect, the identified model suffers from a lack of accuracy due to the residual phase error.

Ku *et al.* [9] presented a parallel Wiener system that established a behavioral model for RF power amplifiers with memory. The model parameters are extracted using two-tone intermodulation-distortion measurements with different tone frequency spacings and power levels. The authors claimed that this model is able to predict accurately ACPR levels close to the carrier frequency for high-power amplifiers. Recently, Jantunen *et al.* [10] developed a nonlinear model with memory based on the Hammerstein structure (static nonlinearity + linear filter) to predict the behavior of a power amplifier for a fourth-generation mobile communications system. They employed a polynomial model for the nonlinearity and a finite impulse response (FIR) filter with a bulk delay for the linear component. However, the model is extracted based on single-tone measurement data instead of realistic modulated signal data. Even though a satisfactory result was reported for the single-tone test signal, its performance under modulated signals is unknown.

The common difficulty for the previous models is in the identification procedure of the parameters of their different modules. The above-mentioned models and procedures encounter high complexity and/or low accuracy. In most cases, they are not appropriate for implementation in adaptive communications systems.

In this paper, a new augmented Weiner model that is capable of accurately modeling wide-band RF transmitters in a 3G context, as well as its related identification procedure, is presented. The remainder of this paper is organized as follows. Section II briefly depicts the wide-band RF transmitter prototype used in this study. Section III explicates the newly proposed procedure and method to deembed the strong nonlinearity from the transmitter response and to identify and quantify accurately the memory effects originally exhibited by the transmitter [11]. The identification procedure and the algorithm then needed to identify the parameters of the Wiener nonlinear system chosen to model wide-band RF transmitters are explained in detail. In Section IV, an accurate time-delay estimation procedure, which is needed for modeling purposes in the context of broad-band transmitters, is presented to precisely align the in-phase (I) and quadrature (Q) streams at the input and output of the transmitters. Section V introduces and verifies an elaborate validation method, in terms of annulling the spectrum regrowth caused by the static nonlinearity, so as to validate the performance of the Wiener models in the prediction of memory effects. In Section VI, a new comprehensive memory-effect model is proposed. This model is able to account for linear distortion (frequency response near the carrier) and weak nonlinear distortion due to baseband frequency response, harmonic loading conditions, and trap effects that might occur in semiconductor devices. Based on this new memory-effect model, an augmented Wiener model is established and found to be much more accurate than the conventional Wiener model in predicting ACPR levels of a wide-band 60-W peak-envelope-power (PEP) GaAs field-effect-transistor (FET) push–pull amplifier-based transmitter driven by multicarrier wide-band code-division multiple-access (WCDMA) signals. Section VII gives the description of the test bed used in the experimental validation of the different models involved in this paper. Finally, Section VIII is dedicated to the validation of the proposed augmented Wiener model and to the discussion of the measurement results.

Fig. 1. Wide-band RF transmitter prototype.

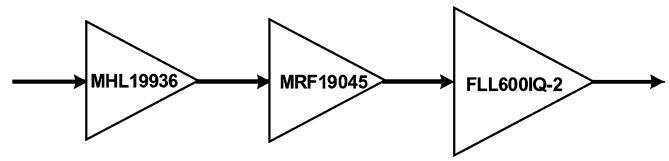

Fig. 2. FLL600IQ-2 PA lineup.

II. Wide-Band RF Transmitter Prototype

As shown in Fig. 1, the wide-band RF transmitter prototype consists of two digital-to-analog converters (DACs), an RF vector modulator, and a power amplifier. The last amplification stage of the power amplifier built for this study, in the band of 1930–1990 MHz, is based on a 60-W PEP push–pull FET transistor (FLL600IQ-2) from Eudyna Devices USA Inc., San Jose, CA [12]. As shown in Fig. 2, a driver amplifier, based on an MRF19045 LDMOS transistor and an MHL19936 gain block, both from Freescale Semiconductor, Austin, TX, is used as the driver stage. The whole lineup has 53-dB gain and 45-dBm saturated power. Furthermore, an electronic signal generator (ESG) (Agilent E4438C) is utilized in this study to emulate the rest of the transmitter. Hence, both the ESG and power amplifier (PA) constitute the transmitter prototype.

It should be pointed out that the PA (last stage) used in this work is based on an FLL600IQ-2 FET transistor, which is of a dual transistor push-pull configuration. This transistor is designed for use in personal-communications-services/networks base station amplifiers instead of the 3G partnership projects (3GPP) base station amplifier. Therefore, the frequency response is relatively poor for 3GPP applications, especially around the center frequency of 1.96 GHz, as can be seen in its datasheet [12]. Moreover, it should be noted that all of the measured transmitter data in the following sections were captured using this transmitter prototype. These data will generally be referred to as transmitter measurements or raw measurement data in the figures of the subsequent sections. Since the output of the memoryless transmitter model only depends on the magnitude of the current input signal, this model is represented by the transmitter amplitude-modulation/amplitude-modulation (AM/AM) and amplitude-modulation/phase-modulation (AM/PM) lookup table model in this work.

Petitioners Exhibit 1004
Page 2 of 10

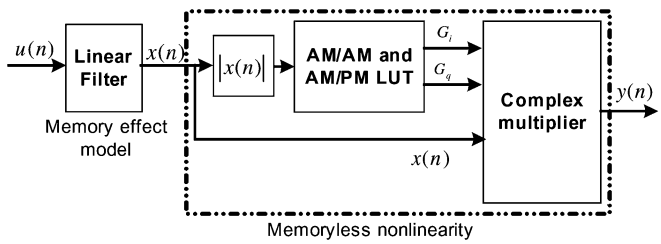

Fig. 3. Wiener transmitter model diagram from [8].

III. Wiener Behavioral Model Construction

A Wiener nonlinear model, shown in Fig. 3, consisting of a dynamic linear filter followed by a static nonlinear block, is adopted to construct a behavioral model of a wide-band RF transmitter. The static nonlinearity can be characterized by the lookup tables based on the AM/AM and AM/PM curves of the transmitter. These curves can be extracted directly from the baseband measurement data by means of a moving average procedure, as explained below. Accordingly, the complex original dynamic nonlinear problem is simplified to a set of linear dynamic problems. In this way, identifying the Wiener nonlinear model becomes easier than the traditional solutions [13], [14], where all of the linear and nonlinear parameters of the Wiener model are resolved concurrently by means of complicated algorithms.

Assuming that the linear filter in Fig. 3 is a FIR filter, then the input and output signals of the two blocks in Fig. 3 can be related as follows:

$$x(n) = \sum_{i=0}^{M-1} a_i u(n-i) \tag{1}$$

$$y(n) = (G_i + jG_q)x(n) = Gx(n) \tag{2}$$

where $G = G_i + jG_q$ denotes the memoryless complex gain of the transmitter that depends only on the instantaneous magnitude of $x(n)$, M stands for the taps of the FIR filter, and a_i are the FIR filter coefficients.

According to (1) and (2), the knowledge of the static nonlinear part of the transmitter model turns the identification of the coefficients a_i of the FIR filter into a simple task. Contrary to previous papers in the literature, the memoryless behavior of the transmitter is represented by a tabulated model (AM/AM and AM/PM) in this work. It allows us to alleviate the burden of the identification procedure of the analytical model's parameters, such as the high-order (even and odd) polynomial function's coefficients [15] and the Bessel series model's coefficients [7], particularly when the power amplifier (PA) operates in class AB. Therefore, this modeling approach is robust, and it is independent of the PA technology and its operation class.

A. Static Nonlinearity Deembedding With Dynamic Exponentially Weighted Moving Average

Given the instantaneous measurements of the I and Q input and output waveforms of the transmitter, the dynamic AM/AM and AM/PM characteristics are first plotted. These plots are assessed under a two-carrier WCDMA signal, which is synthesized according to 3GPP test model 3 with a separation of 5 MHz [16]. Figs. 4 and 5 give evidence of the significant dispersion of the AM/AM and AM/PM curves of the current transmitter and consequently confirm the presence of important memory effects. As a result, the construction of the corresponding model, which is capable of predicting transmitter behavior, necessitates the identification of the parameters of the two blocks shown in Fig. 3. To extract the transmitter static nonlinearity, an exponentially weighted moving average is applied to the dynamic AM/AM and AM/PM data to remove the dispersion. The exponentially weighted moving average algorithm is based on the following equation:

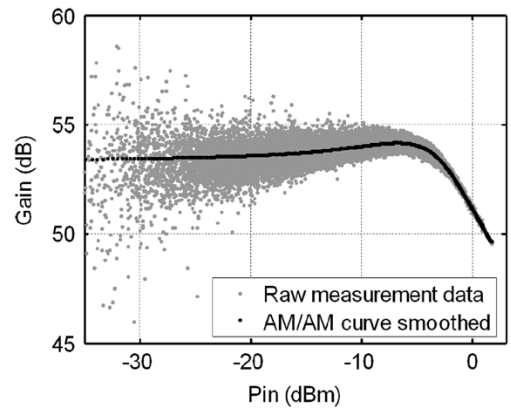

Fig. 4. Smoothed AM/AM curve versus the raw measurement AM/AM data of the transmitter prototype.

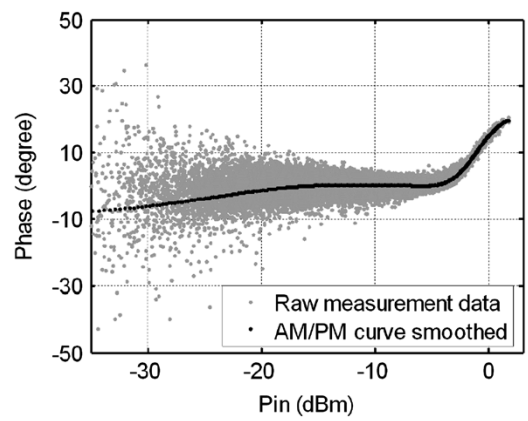

Fig. 5. AM/PM curve smoothed versus the raw measurement AM/PM data of the transmitter prototype.

$$y(n) = \alpha y(n-1) + (1-\alpha)x(n) \tag{3}$$

where α is the weight factor with a value from 0 to 1.

Consider the significant dispersion in the AM/AM and AM/PM characteristics of the transmitter, a fixed α over the input signal dynamic range will lead to a poor moving average quality. In fact, a large value of α will produce smooth (no dispersion), but incorrect traces because of the average error propagation. Similarly, a small value of α ends with a jagged curve. Consequently, to adapt a α's value to the AM/AM and AM/PM variation, a dynamic setting of α is essential. For that reason, the α's value must be expressed as a function of the input power, i.e., $\alpha = F(|x(n)|^2)$.

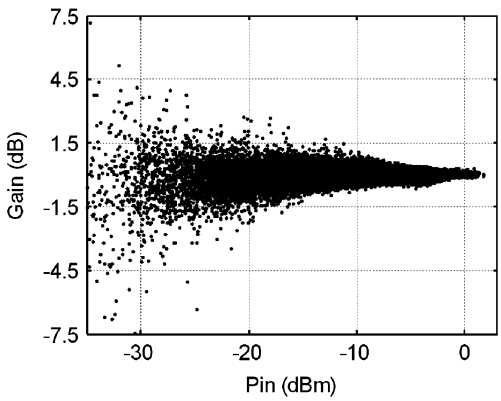

Fig. 6. Dynamic AM/AM characteristics of the linear filter extracted from the measurement data of the transmitter prototype.

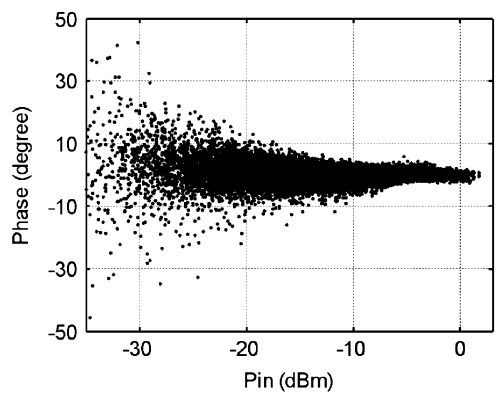

Fig. 7. Dynamic AM/PM characteristics of the linear filter extracted from the measurement data of the transmitter prototype.

The lookup table entries are determined from the AM/AM and AM/PM curves of the transmitter obtained by smoothing the dynamic characteristics using this exponentially weighted moving average. These entries encompass the in-phase and the quadrature components (G_i and G_q) of the complex compression gain corresponding to different magnitude values of $x(n)$.

B. Identification and Modeling of Memory Effects

1) Memory-Effect Identification: The identification of the static nonlinear model on the basis of the dynamic characteristics of the transmitter allows us to fulfill the measured variables listed in Fig. 3. Indeed, the identification of the memory-effect model necessitates the time records of $u(n)$ and $x(n)$, but transmitter characterization does not provide access directly to $x(n)$. In this way, the memoryless block initially identified will be utilized to deduce the time record of $x(n)$ on the basis of the output time record $y(n)$. Therefore, an inverse function of the static nonlinear model is numerically constructed and applied to the measured output signal $y(n)$ in order to get the dynamic linear filter output signal $x(n)$.

2) Modeling of the Linear Distortion: The plot of the AM/AM and AM/PM characteristics while considering $u(n)$ as input and $x(n)$ as output, as given in Figs. 6 and 7, indicates the removal of the nonlinearity. Therefore, the complicated original nonlinear modeling problem is simplified to a linear identification problem. In order to avoid the potential instability of an infinite impulse response filter, a FIR filter is adopted to construct the dynamic linear model in this paper.

If both lengths of the training sequences $u(n)$ and $x(n)$ are N, then (1) can be rewritten in matrix format as follows:

$$X = AW \tag{4}$$

where

$$X = \left[x(M), x(M+1), \ldots, x(N)\right]^T \tag{5}$$
$$W = [a_0, a_1, \ldots, a_{M-1}]^T \tag{6}$$
$$A = \left[U(M) \quad U(M+1) \quad \cdots \quad U(N)\right]^T \tag{7}$$
$$U = \left[u(n) \quad u(n-1) \quad \cdots \quad u(n-M+1)\right]$$
$$n = M, M+1, \cdots, N. \tag{8}$$

Therefore, the identification of FIR filter weights can be made using the recursive least squares algorithm [17]. Here, the measured $u(n)$ and the deduced $x(n)$ are taken as the input signal and desired signal, respectively. The detailed recursive least squares algorithm statement is given as follows.

At first, $F(n)$, $K(n)$, and $P(n)$ are calculated in terms of the following equations:

$$F(n) = P(n-1)U(n) \tag{9}$$
$$K(n) = \frac{F(n)}{\lambda + U^H(n)F(n)} \tag{10}$$
$$P(n) = \frac{1}{\lambda}\left(P(n-1) - K(n)U^H(n)P(n-1)\right) \tag{11}$$

where $P(n)$ is an $M \times M$ matrix. Both $F(n)$ and $K(n)$ are $M \times 1$ matrices. λ is a scalar and denotes the forgetting factor. The output $x_1(n)$ of the filter at the current instant is then

$$x_1(n) = W^H(n-1)U(n). \tag{12}$$

Thus, the output error of the dynamic filter at the current instant is

$$e(n) = x(n) - x_1(n). \tag{13}$$

Finally, the weights of the dynamic filter are updated by

$$W(n) = W(n-1) + K(n)e^*(n). \tag{14}$$

The recursive least squares algorithm is initialized by setting

$$W(0) = 0 \tag{15}$$
$$P(0) = \delta^{-1}I \tag{16}$$

where δ is a small positive constant and I is the $M \times M$ identity matrix.

IV. Influence of Time Delay on Memory-Effect Identification

The time delay that exists between the input and output baseband data waveforms of the transmitter has to be accurately estimated so as to align input and output I–Q streams prior to identifying the transmitter behavioral model. In fact, the time-

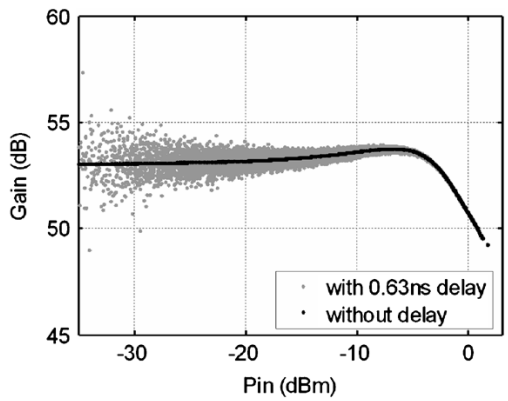

Fig. 8. Simulated AM/AM characteristic comparison between the memoryless models with and without 0.63-ns delay.

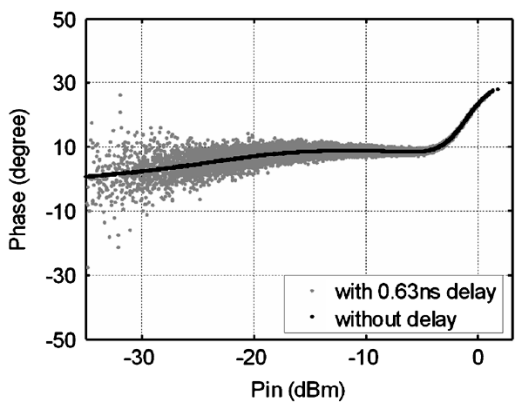

Fig. 9. Simulated AM/PM characteristic comparison between the memoryless models with and without 0.63-ns delay.

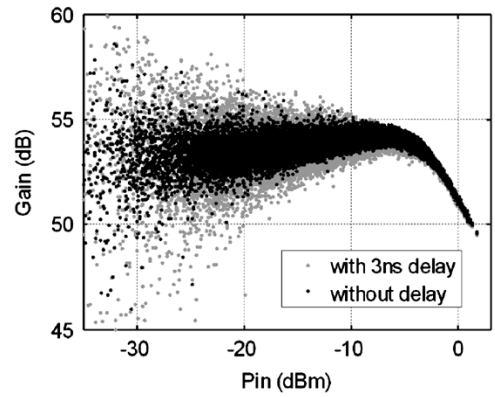

Fig. 10. Measured transmitter AM/AM characteristic comparison with different time delays.

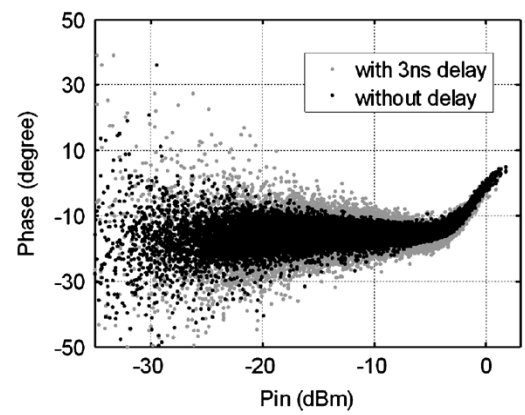

Fig. 11. Measured transmitter AM/PM characteristic comparison with different time delays.

delay estimation becomes more critical when wide-band transmitters are concerned since any time-delay misalignment induces an extra dispersion of AM/AM and AM/PM characteristics of the transmitter. To illustrate the contribution of time delay to the dispersion of AM/AM and AM/PM characteristics of the transmitter, a 0.63-ns delay under a 61.44-mega-sample per second (MSPS) sample rate condition was added while capturing the output of a memoryless transmitter model, which was constructed by the transmitter AM/AM and AM/PM lookup table. The AM/AM and AM/PM characteristics of the memoryless models with and without a 0.63-ns delay are shown in Figs. 8 and 9, respectively. One can clearly observe the dispersion attributed to the time-delay offset. A similar experiment was also carried out to further demonstrate the influence of the time-delay mismatch on memory-effect identification. As shown in Figs. 10 and 11, a 3.0-ns time delay causes strong additional dispersion and scattering in the AM/AM and AM/PM curves. Therefore, inaccurate time-delay estimation and misalignment will conceal the genuine memory effects.

To accurately estimate the time delay between the input sequence $u(n)$ and the output sequence $y(n)$, a cross-covariance of $u(n)$ and $y(n)$ is calculated as follows [18]:

$$C_{xy}(m) = \begin{cases} \sum_{n=0}^{N-m-1}(u(n+m)-\bar{u})(y^*(n)-\bar{y}^*), & m \geq 0 \\ \sum_{n=0}^{N+m-1}(u^*(n-m)-\bar{u}^*)(y(n)-\bar{y}), & m < 0 \end{cases} \tag{17}$$

where N is the length of the sequence. $\bar{u}$ and $\bar{y}$ represent the average values of $u(n)$ and $y(n)$, respectively, which are given by

$$\bar{u} = \frac{1}{N}\sum_{i=0}^{N-1} u(i) \tag{18}$$

$$\bar{y} = \frac{1}{N}\sum_{i=0}^{N-1} y(i). \tag{19}$$

Therefore, the time delay can be determined by

$$\tau = m_{\max} \times \frac{1}{f_s} \tag{20}$$

where f_s denotes the sampling rate and $m_{\max}$ is the index of the maximum covariance.

According to (20), the time-delay estimation accuracy is mainly determined by the sample rate f_s. For example, when the sample rate f_s equals 61.44 MSPS, the time resolution is 16.3 ns. However, in practical situations, the time delay of a PA is generally lower than 15 ns. Thus, the resolution is even larger than the time delay caused by the PA. Consequently, this sample rate cannot meet the requirement of time-delay estimation and should be increased. Indeed, the sample rate fully depends on the speed of the analog-to-digital converters (ADCs) of the feedback path. One possible solution to circumvent this limitation is to update the hardware. Nevertheless, this

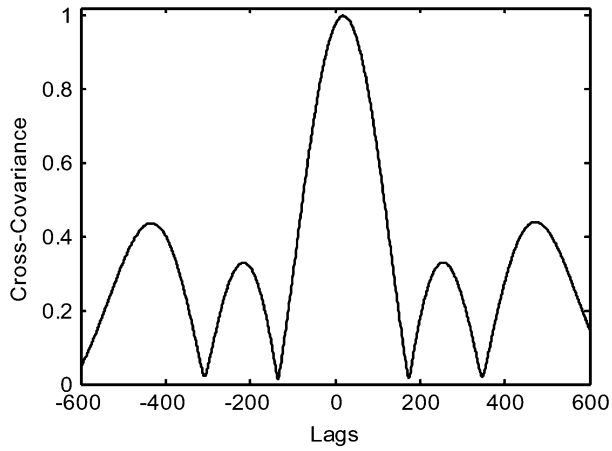

Fig. 12. Cross-covariance calculation results with 15.8-ns delay.

solution is not always possible due to the currently available ADC speed, as well as related expenses. An alternative solution is to use digital signal processing (DSP) techniques. The Lagrange interpolation [19] has, therefore, been adopted in this study to increase the sample rate by 20–30 times. Finally, a higher resolution can be obtained and a satisfactory time-delay estimation achieved. The cross-covariance calculation results with a 26× interpolation for a two-carrier WCDMA signal are shown in Fig. 12. It is clear that the maximum cross-covariance can be found easily and accurately.

It should be pointed out that this time-delay estimation method will use more resources and take longer processing times while having a higher rate interpolation under long time-delay conditions. To overcome this shortcoming, a two-step strategy is adopted for practical implementation. In the first stage, coarse time-delay estimation is performed without interpolation. In the second stage, fine time-delay estimation is carried out by having a higher interpolation rate on a very short data sequence.

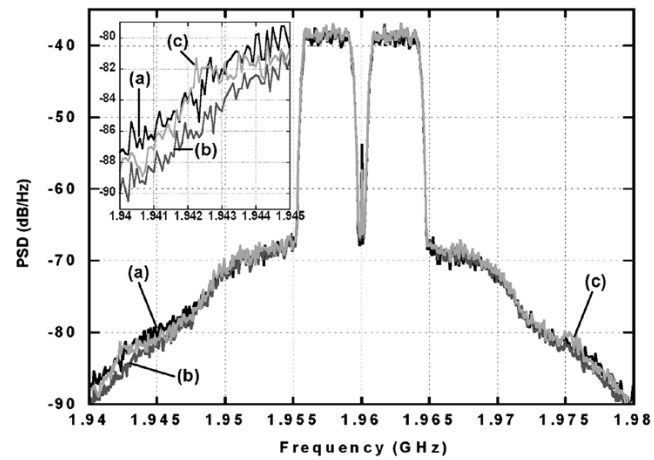

(A)

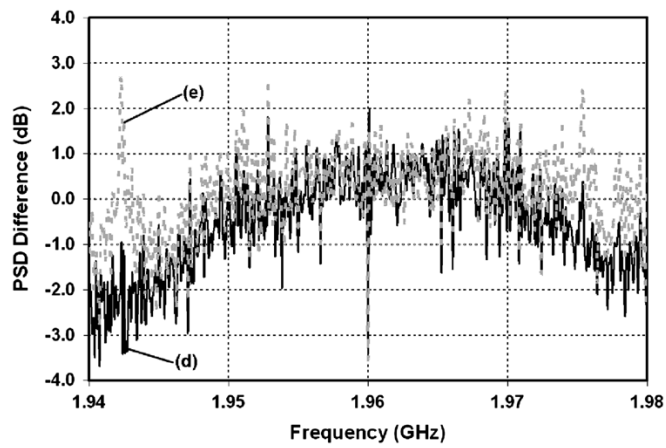

(B)

Fig. 13. Spectrum comparison among the spectra of memoryless model, 64-tap Wiener model, and transmitter measurement. (a) Transmitter measurement. (b) Memoryless model. (c) Wiener model with a 64-tap FIR filter. (d) Spectrum differences between the memoryless transmitter model and the actual transmitter. (e) Spectrum differences between the 64-tap Wiener transmitter model and the actual transmitter.

V. Wiener Model Validation and Limitation Assessment

A. Wiener Transmitter Model Validation Method

The validation of the Wiener model, which is identified using the procedure explained above, was initially carried out through a comparison of the output spectra obtained from the actual transmitter-under-test, the memoryless transmitter model, and the Wiener transmitter model, where a two-carrier WCDMA signal was applied directly to the two transmitter models and to the transmitter prototype. According to Fig. 13(A), the Wiener transmitter model with a 64-tap FIR filter produced an output spectrum that seemed to be close to the measured one. However, to further investigate this matter, the spectrum differences between the two transmitter models and the actual transmitter are illustrated in Fig. 13(B). From this figure, one cannot assert that the Wiener transmitter model performs better than the memoryless transmitter model.

At first glance, such a result seems ambiguous. In fact, the strong static nonlinearity of the transmitter dominates most parts of the emergence of the out-of-band spectrum emission at the transmitter and the model outputs. Consequently, the spectrum regrowth caused by the memory effects is obscured by the spectrum emission produced by the static strong nonlinearity. The contribution of the memory effects in the spectrum regrowth acts as a kind of perturbation; therefore, with such a validation approach, it is very difficult to distinguish the influence of the memory effects on the spectrum regrowth. For that reason, a more appropriate approach has to be applied in order to prove the superiority of the Wiener model over the memoryless behavioral model in mimicking the memory effects of wide-band transmitters.

As mentioned earlier, the Wiener model consists of a dynamic linear block and a static nonlinear block. Thus, a pre-compensation of the static nonlinearity of the transmitter by applying its inverse function permits the decoupling of the out-of-band emission, which is caused by the memory effects, and the spectrum regrowth resulting from the memoryless nonlinearity. In this way, the spectrum regrowth produced by the static nonlinearity is numerically removed from the output spectrum of the transmitter. As a result, the output spectrum observed in the

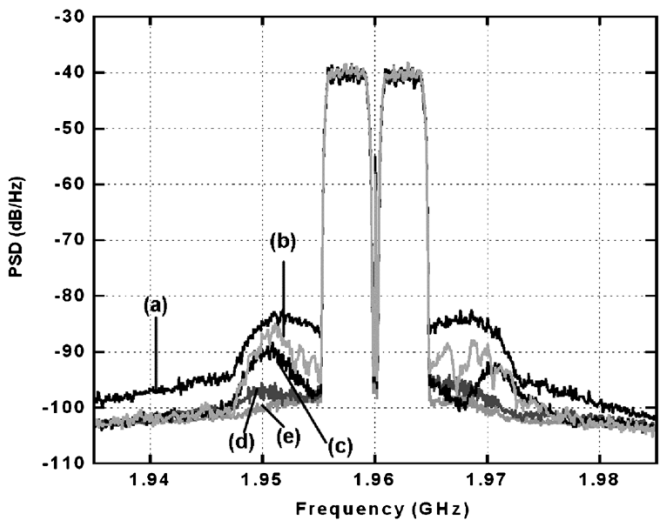

Fig. 14. Spectrum comparison of different Wiener transmitter models and the transmitter prototype. (a) Transmitter measurement. (b) Wiener model with a 64-tap FIR filter. (c) Wiener model with a ten-tap FIR filter. (d) Wiener model with a five-tap FIR filter. (e) Memoryless model.

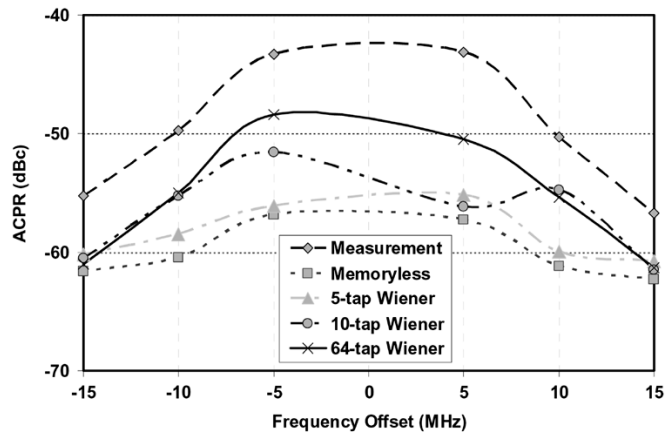

Fig. 15. ACPR comparison of different Wiener transmitter models and the transmitter prototype.

spectrum analyzer is strongly dominated by the memory effects of the wide-band RF transmitter.

With this new model validation method, the output spectrum of the transmitter memoryless model will be almost free of spectrum regrowth. However, the Wiener model and the transmitter prototype output spectrum will include a spectrum regrowth, which can be attributed to the memory effects.

B. Wiener Model Validation

For the purpose of the validation of the Wiener transmitter model, a 1024-entry lookup table and FIR filters with different numbers of taps were constructed by using the I and Q components of the input and output signals of the transmitter. As mentioned earlier, the lookup table was constructed first by using the proposed static nonlinearity deembedding procedure with MATLAB software. The recursive least-squares algorithm was then applied to determine the weights of the FIR filter. The constructed Wiener model was implemented in Agilent Advanced Design System (ADS) for validation purposes. It is worth noting that, in order to check the generality of the Wiener model, a frame of a WCDMA signal different from that used in the model identification step was applied during the validation phase.

Fig. 14 illustrates the capacity of the Wiener models to predict the output spectrum of the transmitter. Here, the transmitter and Wiener models were cascaded with the inverse of the static nonlinearity block. Compared with the measurement spectrum, the Wiener model with a 64-tap FIR filter allows for better prediction of the output spectrum of the transmitter than the Wiener models using five- or ten-tap FIR filters. Furthermore, ACPRs for the different Wiener models and the transmitter prototype output were assessed at several frequency offsets (-15, -10, -5, 5, 10, and 15 MHz) from the center frequency within 3.84-MHz bandwidth, as shown in Fig. 15. ACPR results also demonstrated that the Wiener model with 64-tap FIR filter produced the best results among the three different Wiener models. However, a relatively large difference between the spectrum of the 64-tap Wiener model and the spectrum of the transmitter prototype still existed, especially with the out-of-band spectrum components nearby the two main channels. Therefore, one can conclude that the Wiener model cannot accurately predict the memory effects of the actual wide-band transmitter used in 3G applications.

VI. Augmented Wiener Behavioral Model

A. Inclusive Memory-Effect Model

The memory-effect sources of an RF transmitter are usually attributed to thermal and/or electrical dispersion effects. In the context of a wide-band transmitter, electrical memory effects are the dominant sources of dispersion since the thermal time constant is too large compared to the inverse of the signal bandwidth [20]. Vuolevi *et al.* [21], Ku and Kenney [22] and Remley *et al.* [23] attributed the electrical memory effects to different sources including: 1) trapping effects; 2) impact ionization; 3) the frequency response of the PA around the carrier frequency; 4) matching conditions at harmonic frequencies; and 5) the impedance-matching conditions at the envelope frequency (bias circuit design). The effects of the last two sources are responsible for extra odd-order intermodulation-distortion vectors. Indeed, even-order nonlinearities after remixing with the carrier frequencies lead to odd-order intermodulation products, which are in or very close to the main channel.

The linear FIR filter in the Wiener model, as previously presented, takes into account the frequency response around the carrier frequency (linear distortion) and not the nonlinear even-order distortion sources. In fact, the extracted AM/AM and AM/PM characteristics of the dynamic memory-effect model, as shown in Figs. 6 and 7, are not completely symmetric around the X-axis. This suggests that weak nonlinearities still exist even after deembedding static and strong nonlinearity from the measured data. For this reason, it is not sufficient to model these weak nonlinearities with a linear filter, as is normally done in conventional Wiener models. This also explains the relatively limited capability of the conventional Wiener model to predict the response of the transmitter.

In this paper, a new comprehensive memory-effect model is proposed. As shown in Fig. 16, one can see that a new parallel branch is added to the linear FIR filter. In this new parallel branch, the input signal $u(n)$ is multiplied by its magnitude

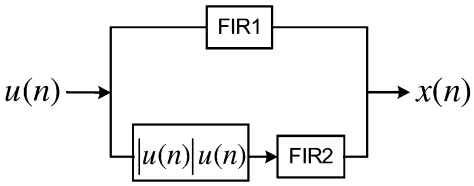

Fig. 16. Dynamic memory-effect model.

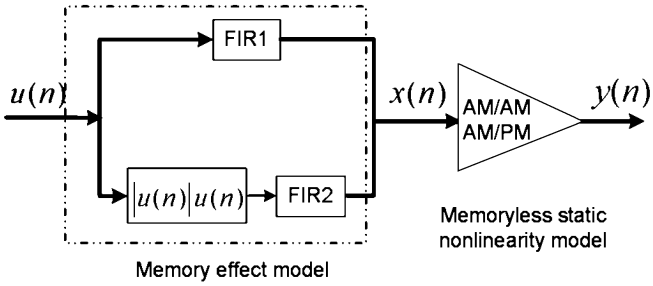

Fig. 17. Augmented Wiener transmitter model diagram.

$|u(n)|$ and applied to another FIR filter. In this way, the linear FIR filter in the conventional Wiener model, as described in Section V, is replaced by a weak nonlinear dynamic FIR-based filter. The second-order terms are introduced to the dynamic memory-effect model in such a way as to make it able to mimic memory effects more accurately.

Using the new inclusive memory-effect model, an augmented Wiener model, as given by Fig. 17, is proposed to model wide-band RF transmitters accurately. This augmented Wiener model is a cascade of a dynamic weak nonlinear model and a strong nonlinear static model. The strong nonlinear model, based on the smoothed AM/AM and AM/PM characteristics of the transmitters, is normally implemented by using lookup tables. The dynamic weak nonlinear model is composed of the new inclusive memory-effect model, which takes into account the dynamic properties of the transmitters in the presence of the modulated communications signal.

B. Augmented Wiener Model Identification

Assuming that the two FIR filters have M_1 and M_2 taps, respectively, the input signal $u(n)$ and output signal $x(n)$ of the dynamic filter block in Fig. 17 can be written as follows:

$$x(n) = \sum_{i=0}^{M_1-1} a_i u(n-i) + \sum_{i=0}^{M_2-1} b_i |u(n-i)| u(n-i) \quad (21)$$

where M_1 and M_2 denote the memory depth of the model. Equation (2) can also be used for the identification of the augmented Wiener model. After removing the strong static nonlinearity using (2), the identification of the coefficients a_i and b_i of the nonlinear filter can be simplified. Let

$$v(n-i) = |u(n-i)| u(n-i). \quad (22)$$

Equation (21) can then be rewritten as

$$x(n) = \sum_{i=0}^{M_1-1} a_i u(n-i) + \sum_{i=0}^{M_2-1} b_i v(n-i). \quad (23)$$

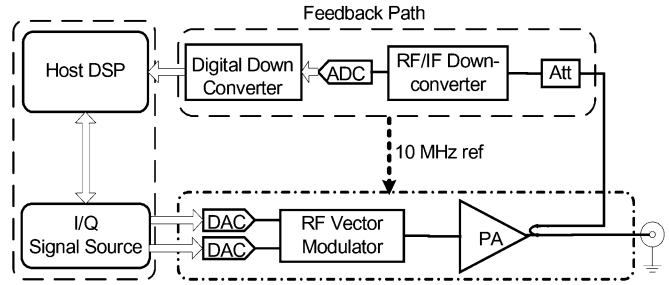

Fig. 18. Wide-band RF transmitter characterization platform.

Consequently, (23) can be solved with a recursive least squares algorithm if (6) and (8) are modified as follows:

$$\begin{aligned} W &= \left[a_0, a_1, \ldots, a_{M_1-1}, b_0, b_1, \ldots, b_{M_2-1}\right]^T \quad (24) \\ U &= \left[u(n), u(n-1), \ldots, u(n-M_1+1),\right. \\ &\quad \left. v(n), v(n-1), \ldots, v(n-M_2+1)\right] \\ n &= M, M+1, \ldots, N \\ M &= \max(M_1, M_2) \quad (25) \end{aligned}$$

where M is the larger one of M_1 and M_2. Since only the first- and second-order terms of the input signals are included in this new model, the algorithm has good numerical stability.

VII. Experimental Setup and Newly Proposed Model Validation

The wide-band RF transmitter characterization platform used in this study is shown in Fig. 18. A PC was utilized as the host DSP to synthesize the test signal and to capture the feedback signal. The I/Q signal source was initially synthesized using Agilent ADS and the arbitrary waveform generator in the ESG. The test signal had two neighboring WCDMA carriers (carrier spacing: 5 MHz), which were configured according to a 3GPP test model 3 with 32 code channels [16]. The test signal synthesized using the ADS 3GPP library had a crest factor of 7.96 dB. The dynamic link between ADS and the ESG was utilized for dynamically uploading the test signal from the host DSP to the I/Q arbitrary waveform generator of the ESG. The signal was then modulated and up-converted to an RF carrier in the ESG, and the RF output of the ESG was fed to the PA.

Having the baseband input waveform directly recorded in the host DSP during the signal synthesis step, the baseband waveform at the output of the transmitter was captured by an RF receiver. This receiver consisted of an RF/IF down-converter, a high-speed ADC, a digital down-converter, and the host DSP, as shown in Fig. 18. In this study, the receiver prototype was physically formed by a spectrum analyzer (Agilent E4446A), a vector signal analyzer (VSA) (Agilent 89611A), and a PC. The Agilent E4446A spectrum analyzer, which was fed with the output RF signal of the PA, translated the RF signal to a 70-MHz IF. The IF signal was then digitized by means of the high-speed digitizer module (Agilent 1439C) and was down-converted to baseband I and Q signals. Finally, the baseband I and Q data were sent to the PC through a high-speed IEEE1394 interface for further processing. The delay calibration function of the VSA was employed to compensate for the time delay caused by the group delay of the transmitter and the output waveform acquisition subsystem.

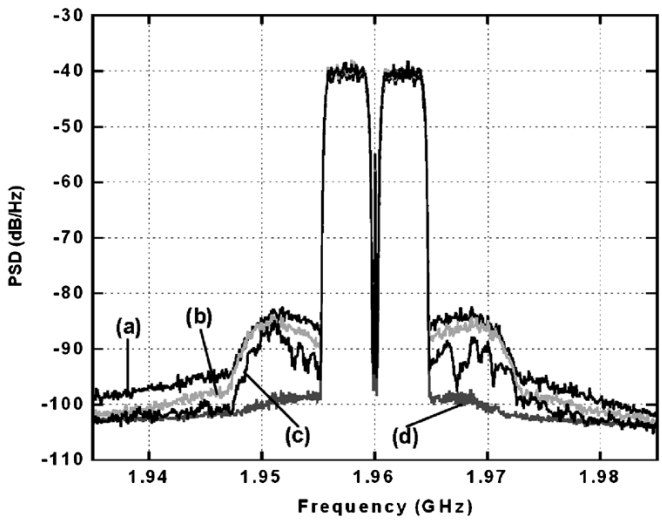

Fig. 19. Spectrum comparison of different transmitter models and the transmitter prototype. (a) Transmitter measurement. (b) Augmented Wiener model with two three-tap FIR filters. (c) Wiener model with a 64-tap FIR filter. (d) Memoryless model.

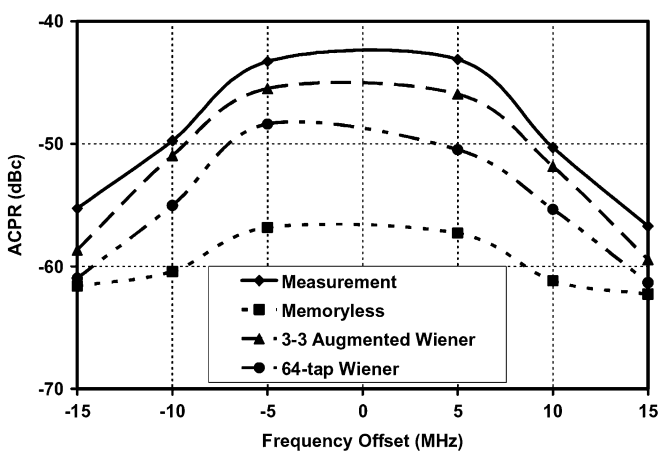

Fig. 20. ACPR comparison of different transmitter models and the transmitter prototype.

VIII. Validation Results and Discussion

As suggested earlier, the validation of the newly proposed model was carried out by preceding the transmitter with its memoryless nonlinear inverse function. Thus, one can concentrate on the capability of the new model in predicting memory effects. For that reason, the identification of the augmented Wiener model parameters was firstly performed according to the method explained in Section VI. A 1024-entry lookup table was constructed, and two three-tap FIR filters were subsequently identified. To illustrate the improved accuracy of this new model, the results obtained previously with the 64-tap Wiener model and the memoryless transmitter model were used as references in the validation process. Both the spectrum comparison results shown in Fig. 19 and the ACPR comparison results shown in Fig. 20 indicate that the augmented Wiener model can predict the memory effects of the transmitter more accurately than the conventional Wiener model. As expected, the memoryless transmitter model cannot predict the memory effects of the wide-band transmitter at all.

IX. Conclusion

In this paper, a nonanalytical modeling technique for the memoryless static nonlinear behaviors of RF transmitters based on a dynamic exponential weighted moving average algorithm has been developed and validated. This technique is inherently so robust that it can be used for any type of RF transmitters exhibiting any complex gain shape variations. In order to deduce an intermediate set of data that could be used in the identification of the dynamic (memory effects) sub-model of the Wiener model, the resulting memoryless AM/AM and AM/PM characteristics have been utilized to deembed the raw measurement data. Subsequently, to identify the memory effects accurately, a time-delay estimation algorithm based on Langrage interpolation and cross-covariance calculation has been developed to align the input and output raw baseband data captured beforehand.

Moreover, to evaluate the accuracy and robustness of the different Weiner models, a novel validation method has been proposed. This method is based on annulling the spectrum regrowth that is caused by static nonlinearity with the help of cascading the inverse of the complex memoryless model. To improve the relatively limited accuracy of the conventional Wiener model, an augmented Wiener model has been proposed, where the linear FIR filter is replaced with a weak nonlinear filter structure. To the best of the authors' knowledge, this is the first time such a nonlinear model has been presented and implemented in practical applications. Finally, the effectiveness of the proposed augmented Wiener model and its identification procedure was assessed using a 60-W PEP GaAs FET push–pull amplifier-based transmitter driven by a two-carrier WCDMA signal. The spectrum comparison results between the different transmitter models and the transmitter prototype reveal that the proposed augmented Wiener transmitter model outperforms other models in predicting the spectrum regrowth caused by the memory effects of the wide-band transmitter.

Acknowledgment

The authors would like to acknowledge J. Gauthier, S. Dube, R. Brassard, R. Archambault, J.-S. Décarie, M. Helaoui, and H. B. Naser, all of Ecole Polytechnique of Montréal, Montréal, QC, Canada, for providing technical and software support during measurements.

References

[1] M. Schetzen, *The Volterra and Wiener Theories Nonlinear Systems*. New York: Wiley, 1980.

[2] A. Zhu, M. Wren, and T. J. Brazil, "An efficient Volterra-based behavioral model for wide-band RF power amplifiers," in *IEEE MTT-S Int. Microwave Symp. Dig.*, Philadelphia, PA, Jun. 8–13, 2003, pp. 787–790.

[3] T. Liu, S. Boumaiza, and F. M. Ghannouchi, "Dynamic behavioral modeling of 3G power amplifiers using real-valued time-delay neural networks," *IEEE Trans. Microw. Theory Tech.*, vol. 52, no. 3, pp. 1025–1033, Mar. 2004.

[4] C. P. Silva, A. A. Moulthrop, and M. S. Muha, "Introduction to polyspectral modeling and compensation techniques for wide-band communications systems," in *58th ARFTG Conf. Dig.*, San Diego, CA, Nov. 29–30, 2001, pp. 1–15.

[5] ——, "Polyspectral techniques for nonlinear system modeling and distortion compensation," in *3rd IEEE Int. Vacuum Electronics Conf. Dig.*, Monterey, CA, Apr. 23–25, 2002, pp. 314–315.

[6] S. Boumaiza and F. M. Ghannouchi, "Realistic power-amplifiers characterization with application to baseband digital predistortion for 3G base stations," *IEEE Trans. Microw. Theory Tech.*, vol. 50, no. 12, pp. 3016–3021, Dec. 2002.

[7] C. J. Clark, G. Chrisikos, M. S. Muha, A. A. Moulthrop, and C. P. Silva, "Time-domain envelope measurement technique with application to wide-band power amplifier modeling," *IEEE Trans. Microw. Theory Tech.*, vol. 46, no. 12, pp. 2531–2540, Dec. 1998.

[8] P. Crama and Y. Rolain, "Broadband measurement and identification of a Wiener–Hammerstein model for an RF amplifier," in *60th ARFTG Conf. Dig.*, Washington, DC, Dec. 5–6, 2002, pp. 49–57.

[9] H. Ku, M. D. McKinley, and J. S. Kenney, "Quantifying memory effects in RF power amplifiers," *IEEE Trans. Microw. Theory Tech.*, vol. 50, no. 12, pp. 2843–2849, Dec. 2002.

[10] P. Jantunen, G. Gamez, and T. Laakso, "Measurements and modeling of nonlinear power amplifiers," in *Proc. 6th Nordic Signal Processing Symp.*, Meripuisto, Espoo, Finland, Jun. 9–11, 2004, pp. 328–331.

[11] T. Liu, S. Boumaiza, M. Helaoui, H. Ben Nasr, and F. M. Ghannouchi, "Behavior modeling procedure of wide-band RF transmitters exhibiting memory effects," presented at the IEEE MTT-S Int. Microwave Symp., Long Beach, CA, Jun. 12–17, 2005.

[12] "FLL600IQ-2 *L*-band high power GaAs FET datasheet," Eudyna Devices USA Inc., San Jose, CA, 2004 [Online]. Available: http://www.us.eudyna.com/products/MWpdf/FLL600IQ-2.pdf.

[13] S. L. Lacy and D. S. Bernstein, "Identification of FIR Wiener systems with unknown, noninvertible, polynomial nonlinearities," in *Proc. American Control Conf.*, Anchorage, AK, May 2002, pp. 893–898.

[14] P. Celka, N. J. Bershad, and J. M. Vesin, "Stochastic gradient identification of polynomial Wiener systems: Analysis and application," *IEEE Trans. Signal Process.*, vol. 49, no. 2, pp. 301–313, Feb. 2001.

[15] L. Ding and G. T. Zhou, "Effects of even-order nonlinear terms on power amplifier modeling and predistortion linearization," *IEEE Trans. Veh. Technol.*, vol. 53, no. 1, pp. 156–162, Jan. 2004.

[16] "3GPP Specifications: TS 25.104 v4.5.0, TS 25.141 v4.5.0," GPP, Sophia-Antipolis, France, 2002 [Online]. Available: ftp://ftp. 3 GPP.org/specs/2002-06/Rel-4/25_series/.

[17] S. Haykin, *Adaptive Filter Theory*, 3rd ed. Upper Saddle River, NJ: Prentice-Hall, 1996.

[18] S. J. Orfanidis, *Adaptive Filter Theory*, 2nd ed. Upper Saddle River, NJ: Prentice-Hall, 1996.

[19] R. Séroul, *Programming for Mathematicians*. Berlin, Germany: Springer-Verlag, 2000.

[20] S. Boumaiza and F. M. Ghannouchi, "Thermal memory effects modeling and compensation in RF power amplifiers and predistortion linearizers," *IEEE Trans. Microw. Theory Tech.*, vol. 51, no. 12, pp. 2427–2433, Dec. 2003.

[21] J. H. K. Vuolevi, T. Rahkonen, and J. P. A. Manninen, "Measurement technique for characterizing memory effects in RF power amplifiers," *IEEE Trans. Microw. Theory Tech.*, vol. 49, no. 12, pp. 1383–1389, Dec. 2001.

[22] H. Ku and J. S. Kenney, "Behavioral modeling of nonlinear RF power amplifiers considering memory effects," *IEEE Trans. Microw. Theory Tech.*, vol. 51, no. 12, pp. 2495–2504, Dec. 2003.

[23] K. A. Remley, M. M. P. Schreurs, D. F. Williams, and J. Wood, "Extended NVNA bandwidth for long-term memory measurements," in *IEEE MTT-S Int. Microwave Symp. Dig.*, Fort Worth, TX, Jun. 6–11, 2004, pp. 1739–1742.

Taijun Liu (S'05) received the B.S. degree in applied physics from the China University of Petroleum, Dongying, China, in 1986, the M. Eng. in electrical engineering from the University of Electronic Science and Technology of China, Chengdu, China, in 1989, and is currently working toward the Ph.D. degree at the École Polytechnique de Montréal, Université de Montréal, Montréal, QC, Canada.

From 1989 to 1992, he was a Lecturer with the Chongqing University of Posts and Telecommunications, Chongqing, China. From 1992 to 1998, he was a Senior Engineer with the Information Technology Company, Dianqiangui Petroleum Exploration Bureau, Kunming, China. From 1999 to 2000, he was a Software Engineer with ElectromagneticWorks Inc., Montréal, QC, Canada. Since September 2000, he has been with the École Polytechnique de Montréal. His current research interests are DSP, neural networks, nonlinear modeling and linearization of wide-band transmitters/power amplifiers, and design of ultra-linear high-efficiency intelligent digital transmitters for broad-band wireless and satellite communications systems.

Mr. Liu was the recipient of the 1990 Second-Class Award presented by the Science and Technology Progress Prize of the Ministry of Machine-building and Electronics Industry of China and the 1991 Third-Class Award presented by the National Science and Technology Progress Prize of China.

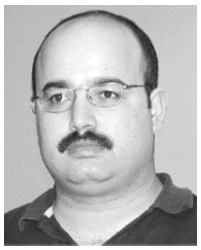

Slim Boumaiza (S'00–M'04) received the B.Eng. degree in electrical engineering from the École Nationale d'Ingénieurs de Tunis, Tunis, Tunisia, in 1997, and the M.S. and Ph.D. degrees from the École Polytechnique de Montréal, Montréal, QC, Canada, in 1999 and 2004.

In May 2005, he joined the Electrical Engineering Department, University of Calgary, Calgary, AB, Canada, as an Assistant Professor and faculty member of the Intelligent RF Radio Laboratory. His research interests are in the general areas of RF/microwave and millimeter components and systems for broad-band wireless and satellite communications. His specific current interests include RF/DSP mixed design of intelligent RF transmitters, design, characterization, modeling and linearization of high-power RF amplifiers, and adaptive DSP.

Fadhel M. Ghannouchi (S'84–M'88–SM'93) received the B.Eng. degree in engineering physics and the M.S. and Ph.D. degrees in electrical engineering from the École Polytechnique de Montréal, Montréal, QC, Canada, in 1983, 1984, and 1987, respectively.

He is currently an iCORE Professor with the Intelligent RF Radio Laboratory, Electrical and Computer Engineering Department, University of Calgary, Calgary, AB, Canada, and Tier-I Canada Research Chair in Intelligent RF Radio Technology. From 1984 to 2005, he was a Professor with the Department of Electrical Engineering, École Polytechnique de Montréal. He has taught microwave theory and techniques and RF communications systems. He held several invited positions at several academic and research institutions in Europe, North America, Japan, and North Africa. He has provided consulting services to numerous microwave and wireless communications companies. He is also the founder of AmpliX Inc., Montréal, QC, Canada, a company that offers linearization products and services to wireless and satellite communication equipment manufacturers. His research interests are in the areas of microwave instrumentation and measurements, nonlinear modeling of microwave devices and communications systems, design of power- and spectrum-efficient microwave amplification systems, and design of intelligent RF transceivers for wireless communications. He has authored or coauthored over 250 publications. He holds seven patents.

Dr. Ghannouchi is a Registered Professional Engineer in the Province of Quebec, Canada. He has served on the Technical Committees of several international conferences and symposiums.